

High-Dimensional Bayesian Optimization via Tree-Structured Additive Models

Eric Han,¹ Ishank Arora,² Jonathan Scarlett^{1,3}

¹School of Computing, National University of Singapore

²Indian Institute of Technology (BHU) Varanasi

³Department of Mathematics & Institute of Data Science, National University of Singapore
eric_han@nus.edu.sg, ishank.arora.cse14@iitbhu.ac.in, scarlett@comp.nus.edu.sg

Abstract

Bayesian Optimization (BO) has shown significant success in tackling expensive low-dimensional black-box optimization problems. Many optimization problems of interest are high-dimensional, and scaling BO to such settings remains an important challenge. In this paper, we consider generalized additive models in which low-dimensional functions with overlapping subsets of variables are composed to model a high-dimensional target function. Our goal is to lower the computational resources required and facilitate faster model learning by *reducing the model complexity* while retaining the *sample-efficiency* of existing methods. Specifically, we constrain the underlying dependency graphs to tree structures in order to facilitate both the structure learning and optimization of the acquisition function. For the former, we propose a hybrid graph learning algorithm based on Gibbs sampling and mutation. In addition, we propose a novel zooming-based algorithm that permits generalized additive models to be employed more efficiently in the case of continuous domains. We demonstrate and discuss the efficacy of our approach via a range of experiments on synthetic functions and real-world datasets.

1 Introduction

Bayesian Optimization (BO) is a widespread method for sequential global optimization (Snoek, Larochelle, and Adams 2012), and is suited to scenarios in which the target function f is unknown and expensive to evaluate. BO was traditionally used in model selection (Moćkus 1975) and hyperparameter tuning (Snoek, Larochelle, and Adams 2012; Swersky, Snoek, and Adams 2013). Recently, BO has also found success in black-box adversarial attack (Ru et al. 2020), robotics (Jaquier et al. 2020), finance (Gonzalez et al. 2019), pharmaceutical product development (Sano et al. 2019), natural language processing (Yogatama, Kong, and Smith 2015), and more. Two critical ingredients of BO include a model that captures prior beliefs about the objective function, and an acquisition function that can be optimized efficiently.

BO has been most successful in low dimensions (i.e. 10 or less) (Wang et al. 2013; Nayebi, Munteanu, and Poloczek 2019), whereas many applications require optimization in higher-dimensional spaces; this remains a critical problem in BO (Wang 2016; Rolland et al. 2018; Frazier 2018).

Copyright © 2021, Association for the Advancement of Artificial Intelligence (www.aaai.org). All rights reserved.

A key difficulty associated with high-dimensional BO is the curse of dimensionality (Spruyt 2014), namely, exponentially many observations are needed to find the global optimum in the absence of structural assumptions. Accordingly, two significant opposing challenges include the incorporation of suitable structural assumptions, and computationally efficient acquisition function optimization.

1.1 Related Work

In the literature, there are at least two approaches to high-dimensional BO with differing assumptions:

- Under *low effective dimensionality*, only few dimensions significantly affect f . (Chen, Castro, and Krause 2012) performed joint variable selection and optimization using GP-UCB. (Djolonga, Krause, and Cevher 2013) applied low-rank matrix recovery techniques to learn the underlying effective subspace, and (Zhang, Li, and Su 2019) proposed a related approach based on sliced inverse regression. (Wang et al. 2013) proposed REMBO, tackling the problem through random embedding. More recently, (Kirschner et al. 2019) proposed LineBO, decomposing the problem into a sequence of one-dimensional sub-problems. The use of *non-linear* low-dimensional embeddings has also recently been proposed (Lu et al. 2018; Moriconi, Kumar, and Deisenroth 2019).
- Under *additive structure*, small subsets of variables interact with each other. Specifically, additive models assume that f can be decomposed into sums of lower-dimensional functions. (Kandasamy, Schneider, and Póczos 2015) assumed that the variables constructing a particular lower-dimensional function are not present in the other decomposed functions (i.e., the variables of each function are pairwise disjoint), which we refer to as Graph No-Overlap. (Rolland et al. 2018) generalized the additive model to allow for an arbitrary dependency graph, removing the restriction of pairwise disjointness, which we refer to as Graph Overlap. Also considering overlapping groups, (Hoang et al. 2018) assumed that f can be decomposed into several sparse factor functions, allowing for distributed acquisition function approximation. (Li et al. 2016) generalized to a projected-additive assumption; the model proposed by (Kandasamy, Schneider, and Póczos 2015) is a special case when there is no projection. Ensemble BO (Wang et al. 2018) seeks to not only exploit addi-

tive structures, but also use an ensemble of GP models through a divide and conquer strategy. (Mutny and Krause 2018) combined additive GPs with approximations based on Fourier features, with the notable advantage of also establishing rigorous regret bounds.

In addition to the methods described above, other approaches have been taken to tackle high dimensionality. (Li et al. 2017) proposed a dropout strategy to optimize on a smaller subset of variables for every iteration. (Oh, Gavves, and Welling 2018) proposed BOCK, which tackles high-dimensionality via a cylindrical transformation of the search space. (Eriksson et al. 2019) proposed an approach based on running several local search procedures in parallel, and giving more samples to the most promising ones. Other methods use deep neural networks combined with BO, such as (Snoek et al. 2015; Cui, Yang, and Hu 2019).

The assumptions of low effective dimension vs. additive structure are complementary. The performance of the optimization is dependent on the structure of the high-dimensional function, and trade-offs exist between computation time and accuracy. Methods that assume low effective dimensionality are often computationally faster than additive methods; for example, due to scalability concerns, (Eriksson et al. 2019) omitted methods that attempt to learn an additive decomposition from their experiments. To the best of our knowledge, none of the existing works have scaled Graph Overlap past 20 to 30 dimension.

In this paper, our focus is on additive structures; in particular, we seek to build on Graph Overlap. Graph Overlap maintains computational tractability by using a message passing algorithm to optimize the acquisition function efficiently. However, the message passing algorithm runs exponentially in the size of the maximum clique of the triangulated dependency graph (Rolland et al. 2018), impeding its scalability.

We see in the above-outlined works (Rolland et al. 2018; Hoang et al. 2018; Li et al. 2016) that the trend in the study of additive models has been to increase the model expressiveness. An important caveat to such approaches is that a suitable model may be *much harder to find* given limited samples. Since one of the main premises of BO is optimizing with few samples, we contend that *simpler* models should also be sought to facilitate model learning with fewer samples, as well as reduced computation.

1.2 Contributions

The main contributions of this paper are as follows:

1. We trade-off expressiveness for scalability and ease of learning by reducing the complexity of the additive model, constraining the dependency structure to tree structures. As the function class is simpler, it reduces overfitting of the GP kernel, and we are also able to reap computational efficiencies in both acquisition function optimization and dependency structure learning.
2. We propose a zooming technique for extending the message passing algorithm of (Rolland et al. 2018) to continuous domains, thus benefiting additive methods in general, and in particular our tree-based approach.
3. We propose a hybrid method to learn the additive tree structures, composed of the following two techniques:

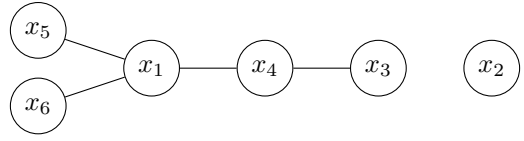


Figure 1: Dependency tree structure, $h(x) = h^A(x_1, x_6) + h^B(x_1, x_5) + h^C(x_1, x_4) + h^D(x_3, x_4) + h^E(x_2)$.

- (a) a tree structure growing algorithm that efficiently discovers edges that do not form cycles via Gibbs sampling;
 - (b) an edge mutation algorithm that obtains a new generation of trees from the current tree efficiently.
4. Although limiting to tree structures may seem potentially risky due to the reduced expressivity, we show this approach to be highly effective in a wide range of experiments, indicating a highly competitive trade-off between expressive power and ease of model learning.

We briefly mention that the use of tree structures in BO appeared in prior works (Jenatton et al. 2017; Ma and Blaschko 2020), but with a very different type of model and motivation. These works aim to handle structured domains instead of real-valued domains, and in contrast with our work, the tree represents binary decisions with only the leaves corresponding to Gaussian Processes.

2 Additive GP-UCB using Tree Structures

We consider the sequential global optimization problem, seeking $x_{\max} = \arg \max_{x \in \mathcal{X}} f(x)$ for a D -dimensional black-box function $f : \mathcal{X} \rightarrow \mathbb{R}$, where $\mathcal{X} = \times_{i=1}^D \mathcal{X}_i$ with each \mathcal{X}_i being an interval in \mathbb{R} . At the t -th observation, the algorithm selects x_t and observes a noisy observation $y_t = f(x_t) + \epsilon_t$, with $\epsilon_t \sim \mathcal{N}(0, \eta^2)$.

2.1 Additive Dependency Tree Structures

We use a Gaussian Process (GP) model to reason about the target function f . Following (Rolland et al. 2018), we model f as a sum of several lower-dimensional components:

$$f(x) = \sum_{G \in \mathcal{G}} f^G(x^G), \quad (1)$$

where $G \subseteq \{1, \dots, D\}$ denotes one subset of variables, and \mathcal{G} represents the additive structure (see Fig. 1 for an example). The additive dependency structure is assumed to be tree-structured, possibly including forests. In contrast with (Rolland et al. 2018), in our setting the additive structure associated with any given graph is unique: Each lower-dimensional component $f^G : \mathcal{X}^G \rightarrow \mathbb{R}$ is either a 1 or 2-dimensional function defined on the variables in G , where $\mathcal{X}^G = \times_{v \in G} \mathcal{X}_v$. Each edge represents a 2-dimensional function, and each disconnected vertex represents a 1-dimensional function.

2.2 Prior and Posterior

We model $f \sim \mathcal{GP}(\mu, \kappa)$, with each f^G being an independent sample from a Gaussian Process $\mathcal{GP}(\mu^G, \kappa^G)$, and

$$\begin{aligned}\mu(x) &= \sum_{G \in \mathcal{G}} \mu^G(x^G), \\ \kappa(x, x') &= \sum_{G \in \mathcal{G}} \kappa^G(x^G, x'^G).\end{aligned}\quad (2)$$

We know from (Rolland et al. 2018) that the posterior can be inferred via $(f_*^G | \mathbf{y}) \sim \mathcal{N}(\mu_{t-1}^G, (\sigma_{t-1}^G)^2)$ for each f_*^G at an arbitrary point x_* given $\mathcal{D}_t = \{(x_i, y_i)\}_{i=1}^t$, where $\mathbf{y} = (y_1, \dots, y_t)$ correspond to $\mathbf{x} = (x_1, \dots, x_t)$, and the posterior mean and variance are given by

$$\begin{aligned}\mu_{t-1}^G &= \kappa^G(x_*^G, \mathbf{x}^G) \Delta^{-1} \mathbf{y}, \\ (\sigma_{t-1}^G)^2 &= \kappa^G(x_*^G, x_*^G) \\ &\quad - \kappa^G(x_*^G, \mathbf{x}^G) \Delta^{-1} \kappa^G(\mathbf{x}^G, x_*^G).\end{aligned}\quad (3)$$

Here we define the matrix $\Delta = \kappa(\mathbf{x}, \mathbf{x}) + \eta^2 I_t \in \mathbb{R}^{t \times t}$, $\kappa(x_i, x_j)$ is the (i, j) -th entry of $\kappa(\mathbf{x}, \mathbf{x})$, and $\kappa^G(\mathbf{x}^G, x_*^G)$ is of length t , with i -th entry $\kappa^G(x_i^G, x_*^G)$.

3 Additive GP-UCB on Tree Structures

Algorithm 1: TREE-GP-UCB

```

1 Initialize  $\mathcal{D}_0 \leftarrow \{(x_t, y_t)\}_{x_t \in X_{\text{init}}}$ 
2 for  $t = N_{\text{init}} + 1, \dots, N_{\text{iter}}$  do
3   if  $t \bmod C = 0$  then
4      $\mathcal{G} \leftarrow \text{LEARN}(\mathcal{D}_{t-1})$  (Alg. 3)
5   Update  $\mu_t^G, \sigma_t^G : \forall G \in \mathcal{G}$  (3)
6   Optimize  $x_t \leftarrow \arg \max_{x \in \mathcal{X}} \phi_t(x)$  (Alg. 2)
7   Observe  $y_t \leftarrow f(x_t) + \epsilon$ 
8   Augment  $\mathcal{D}_t \leftarrow \mathcal{D}_{t-1} \cup \{(x_t, y_t)\}$ 
9 return  $\arg \max_{(x,y) \in \mathcal{D}} y$ 
```

In Alg. 1, we present Tree-GP-UCB (Tree for short). Here, the total number of observations is $N = N_{\text{init}} + N_{\text{iter}}$, where N_{init} is the number of initial random samples X_{init} drawn uniformly from \mathcal{X} and N_{iter} is the number of iterations. For efficiency, \mathcal{G} and its hyperparameters are learned every C iterations, for some $C > 0$.

3.1 Acquisition Function

We focus on upper confidence bound (UCB) based algorithms (Auer 2002; Srinivas et al. 2010). Specifically, following (Kandasamy, Schneider, and Póczos 2015) and (Rolland et al. 2018), we let the global acquisition function $\phi_t(x)$ be the sum of the individual acquisition functions with respect to the dependency structure \mathcal{G} :

$$\begin{aligned}\phi_t(x) &= \sum_{G \in \mathcal{G}} \phi_t^G(x^G), \\ \phi_t^G(x^G) &= \mu_{t-1}^G(x^G) + \beta_t^{1/2} \sigma_{t-1}^G(x^G).\end{aligned}\quad (4)$$

Maximization over Continuous Domains. The message passing approach proposed by (Rolland et al. 2018) works on discrete domains. A naive approach to handle continuous domains would be to discretize the continuous domain uniformly (i.e., a grid with equal spacing). However, this may require large amounts of computation, especially when the discretization is performed using a small spacing. Here, we present a refined message passing algorithm specifically designed for continuous domains.

Algorithm 2: MSG-PASSING-CONTINUOUS

```

1 Initialize  $(\mathbf{a}, \mathbf{b})$  with the bounds of  $\mathcal{X}$ 
2 for  $l = 1, \dots, L$  do
3   for  $d = 1, \dots, D$  do
4     Discretize  $\mathcal{X}_d \leftarrow [[a_d, b_d]]_R$  //  $|\mathcal{X}_d| = R$ 
5    $\mathcal{X} \leftarrow \times_{d=1}^D \mathcal{X}_d$ 
6    $(x, y) \leftarrow \text{MSG-PASSING-DISCRETE}(\mathcal{X})$ 
7   Select  $(\mathbf{a}, \mathbf{b}) \leftarrow \text{ZOOM-STRATEGY}(x)$ 
8 return  $(x, y)$ 
```

The optimization of the acquisition function over continuous domains is presented in Alg. 2; it starts with the full continuous domain $\mathcal{X} = \times_{d=1}^D \mathcal{X}_d$, where $\mathcal{X}_d \in [a_d, b_d] \subseteq \mathbb{R}$. Firstly, we discretize each variable's domain to a finite subset, and let R denote the size of the subset. Thereafter, we use a simplified version of the message passing algorithm MSG-PASSING-DISCRETE of (Rolland et al. 2018)—Alg. S1 in the appendix—to perform optimization over the discretized domain. As the dependency graph is a tree, the complexity of message passing is quadratic in R . The bounds (\mathbf{a}, \mathbf{b}) for the next level are picked by ZOOM-STRATEGY (see below) given the selected point. We perform the steps iteratively for some number L of levels.

Zoom Strategy. Different strategies can be employed in choosing the bounds and their representative points for the next level. We adopt a simple randomized strategy exemplified in Fig. 2: At each level, we partition each current interval $[a_i, b_i]$ uniformly onto a grid of size R , and choose a uniformly random point within that interval as its representative. We refer to this discretization of the domain as $[[a_i, b_i]]_R$. We use MSG-PASSING-DISCRETE restricted to these representatives, and for the one chosen, we recursively zoom into the corresponding sub-domain. Henceforth, we use MSG-PASSING-CONTINUOUS with this zoom strategy.

3.2 Additive Components

The choice of an appropriate kernel and the learning of its parameters are critical to the success of BO. In high-dimensional additive BO, the problem compounds, as we need to learn the dependency structure along with kernel parameters for every kernel in the additive model.

As mentioned previously, an additive decomposition \mathcal{G} corresponds to a dependency graph; the additive function $f(x) = \sum_{G \in \mathcal{G}} f^G(x^G)$ is the sum over its additive components in \mathcal{G} . It will be convenient to work with the equiva-

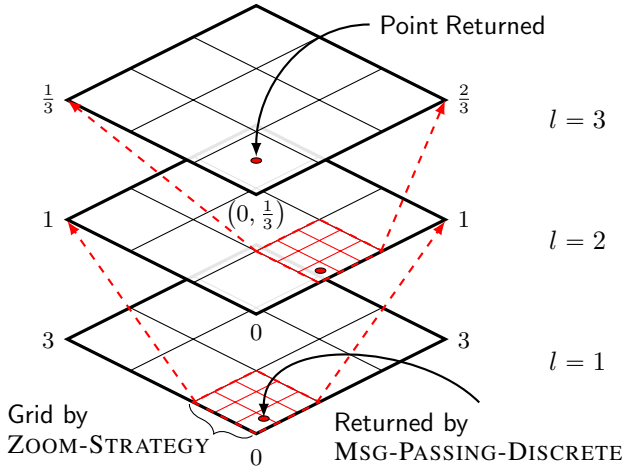


Figure 2: Example with two variables, grid size $R = 3$, and domain $[0, 3]$. Firstly, we partition each axis evenly into 3 partitions. Next, we draw a uniformly random point from each partition. The points from each axis form a discretized domain, and we run MSG-PASSING-DISCRETE on this discrete domain. Finally, we zoom into the square, representative of the selected point. In this manner, we recursively sub-divide the grid for all $L = 3$ levels.

lent representation of an adjacency matrix $Z \in \{0, 1\}^{D \times D}$, where $Z_{ij} = 1$ if variables i and j are connected on the (tree-structured) graph. Assuming that each function’s kernel κ^G is parameterized by some kernel parameters θ^G (e.g., lengthscale etc.), the overall collection of parameters is $\Theta_G = \{\theta^G\}_{G \in \mathcal{G}}$ given a decomposition \mathcal{G} . We note that learning the kernel parameters along with the decomposition \mathcal{G} is difficult, as the search space is large and we may encounter problems with overfitting. We tackle this problem by defining a fixed set of dimensional kernel parameters Θ that are independent of the decomposition and defining the kernel parameters over them; see Sec. 4.1 for details.

Maximum likelihood. For model learning, we make use of the maximum log-likelihood score, given by

$$\rho(Z, \theta) = -\frac{1}{2} \mathbf{y}^T (K + \eta^2 I)^{-1} \mathbf{y} - \frac{1}{2} \log |K + \eta^2 I| - \frac{n}{2} \log 2\pi, \quad (5)$$

where $K \in \mathbb{R}^{n \times n}$ is the kernel matrix of the observed data points n , assuming a dependency graph \mathcal{G} with an equivalent adjacency matrix Z and parameters θ .

Dependency Structure Learning. Following (Wang et al. 2017; Rolland et al. 2018), we adopt a Bayesian approach to structure learning, on which we place a prior distribution on Z and seek to sample from the posterior distribution. We use Gibbs sampling to sample approximately, avoiding the difficult task of sampling directly from the high-dimensional distribution over tree structures.

Specifically, we use such sampling to update the presence/absence of edges from variable i to j , but to maintain the tree structure, we discard edges that would create a cycle. We assume a prior with Bernoulli random variables with parameter γ , $Z_{ij} \sim \text{Bernoulli}(\gamma)$. We can use this model to formulate the posterior for Z_{ij} ; letting \mathcal{D} denote the data collected, and letting $Z_{-(ij)}$ be the adjacency variables excluding (i, j) , we have the following (Rolland et al. 2018):

$$P(Z_{ij} = 1 \mid Z_{-(ij)}, \theta, \mathcal{D}; \gamma) \propto \gamma e^{\rho(Z_{ij}=1 \cup Z_{-(ij)}, \theta)}. \quad (6)$$

For each Z_{ij} , we compare the log of the posterior for two cases: $\log(\gamma) + \rho(Z_{ij} = 1 \cup Z_{-(ij)}, \theta)$ vs. $\log(1 - \gamma) + \rho(Z_{ij} = 0 \cup Z_{-(ij)}, \theta)$. The parameter γ can be set to $1/2$ if there is no prior information about Z . We use the log-likelihood in two ways, combining them to learn the structure in Alg. 3. First, we use Gibbs Sampling to build a connected tree from an empty graph iteratively. Once the dependency graph is a connected tree, we apply mutation in subsequent iterations. Thus, we grow the empty graph into a tree and then seek improvements via mutation.

Algorithm 3: TREE-LEARNING

```

1  $\mathcal{Z} \leftarrow \{Z^{\text{current}}\}$ 
2  $Z^{(k)} \leftarrow Z^{\text{current}}$ 
3 while  $k < S$  do
4   if  $\text{NUMBER-OF-EDGES}(Z^{(k)}) < D - 1$  then
5      $\text{Update}(\mathcal{Z}, k)$  via GIBBS-SAMPLING (Alg. 4)
6   else
7      $\text{Update}(\mathcal{Z}, k)$  via MUTATION (Alg. 5)
8 return  $Z \in \mathcal{Z}$  with the highest likelihood score
```

Adding Edges. Alg. 4 samples from the marginal posteriors, while only adding edges that maintain that Z is still a tree. The Union-Find (UF) data structure tracks a set of disjoint sets, providing the operations *union* and *find*. Both operations can be performed in (amortized) time $O(\alpha(D))$ when implemented using weights with path compression (Cormen et al. 2009; Sedgewick and Wayne 2011), where $\alpha(D)$ is the inverse Ackermann function. In short, both operations can be performed in nearly constant time (amortized). In our algorithm, we use UF to track the connected components of \mathcal{G} , represented by disjoint subsets of variables. We use the *find* operation to check for cycles. After adding the edge, we update UF by performing the *union* operation.

Mutation. Alg. 5 describes the mutation operation that we perform when the dependency graph \mathcal{G} is a connected tree. We borrow the idea of mutation from genetic algorithms; the mutation operation can maintain tree structure diversity from one generation to another. The purpose of the mutation operation is to preserve and introduce diversity, wherein genetic algorithms, a mutation helps to avoid getting stuck in local maxima by making minor changes to the previous generation. In our context, the population is a new generation of trees in

Algorithm 4: GIBBS-SAMPLING at k -th iteration

```
1 Initialize UF data structure
2 for  $j = 1, \dots, D$  do
3   for  $i = 1, \dots, j - 1$  do
4      $Z^{(k+1)} \leftarrow Z^{(k)}$ 
5     if cycle not formed by  $Z_{ij}^{(k+1)} = 1$  then
6       Sample  $Z_{ij}^{(\text{new})}$  from posterior
7        $Z^{(k+1)} \leftarrow Z_{ij}^{(\text{new})}$ 
8       Update UF via union operation
9       Add  $\mathcal{Z} \leftarrow \mathcal{Z} \cup \{Z^{(k+1)}\}$ 
10   $k \leftarrow k + 1$ 
```

each iteration, and the fitness function is the log-likelihood. Using mutation, we can simultaneously avoid local maxima and efficiently maintain a tree structure.

We note that one could simply use the Gibbs sampling approach or the mutation approach separately rather than using the former followed by the latter, but we found this combined approach to be effective experimentally.

Algorithm 5: MUTATION at k -th iteration

```
1  $Z^{(k+1)} \leftarrow Z^{(k)}$ 
2  $i, j \leftarrow$  Sample random edge for which  $Z_{ij}^{(k+1)} = 1$ 
3 Remove edge:  $Z_{ij}^{(k+1)} = 0$ 
4  $i', j' \leftarrow$  Sample nodes from the disconnected sub-trees
5 Sample  $Z_{i'j'}^{(\text{new})}$  using posterior
6  $Z^{(k+1)} \leftarrow Z_{i'j'}^{(\text{new})}$ 
7 Augment the dataset:  $\mathcal{Z} \leftarrow \mathcal{Z} \cup \{Z^{(k+1)}\}$ 
8  $k \leftarrow k + 1$ 
```

4 Experimental Results

For each of our experiments,¹ we compare our method, Tree, to several state-of-the-art black-box global optimization methods, particularly BO methods including Graph No-Overlap (Kandasamy, Schneider, and Póczos 2015), Graph Overlap (Rolland et al. 2018), LineBO (Kirschner et al. 2019), and REMBO (Wang et al. 2013).

To avoid clutter, we avoid including every algorithm and baseline in our charts. Instead, we make an effort to compare against the *best* algorithm for the function at hand, leveraging on prior works’ experimental results to complete our discussion. For example, in cases where LineBO was already shown to outperform standard GPs and REMBO in (Kirschner et al. 2019), we omit these worse-performing methods.

We run all additive methods using the zooming-based message passing algorithm, analogous to Alg. 2. In addition, we compare to Random, which evaluates points at random.

¹The code is available at <https://github.com/eric-vader/HD-BO-Additive-Models>.

Where possible, we also compare our results to Oracle, which has access to the true dependency graph along with the true kernel parameters. The functions and data sets considered are summarized in Table S2 in the appendix.

4.1 Setup

Whenever possible, we used identical parameters across all competing algorithms and functions. However, we note that most algorithms have unique hyperparameters. We set those hyperparameters to reasonable values, discussed in the appendix. The competing algorithms and their unique hyperparameters are given in Table S1 in the appendix. We ran each algorithm 25 times for every function with varied conditions.² We ran all experiments with $N_{\text{init}} = 10$ initial points and $N_{\text{iter}} = 1000$ total points. The same conditions are used across all algorithms to ensure a fair comparison.

Kernel. We adopt the widely-used Radial Basis Function (RBF) kernel, more specifically using a variant known as the RBF-ARD kernel (Murphy 2012), which consists of a dimensional lengthscale ℓ_i for every dimension i . In addition, we decompose the scale parameter $\sigma^G = \sqrt{\sum_{i \in G} \sigma_i^2}$ into its dimensional components σ_i , so that we can learn the parameters tractably. Each low-dimensional kernel corresponds to a low-dimensional function with set of variables G :

$$\kappa_{\text{RBF}}^G(x, x') = \sigma^G \exp \left(-\frac{1}{2} \sum_{i \in G} \frac{(x_i - x'_i)^2}{\ell_i^2} \right). \quad (7)$$

In this manner, the kernel parameters Θ_G are defined over the dimensional kernel parameters $\Theta = \{(\ell_i, \sigma_i)\}_{i=1}^D$. We adopt the established gradient-based approach to learning Θ ; see Sec. S1 in the appendix. We initialize the dimensional lengthscale and scale parameters as $\sigma_i = 0.5$, and $\ell_i = 0.1$ for all i . We set $\eta = 0.1$ in (3) to account for noisy observations.

Additive Models. All additive models start with an empty graph of the appropriate size for the given function. Concerning the learning of the dependency structure, we assume no prior knowledge ($\gamma = 0.5$). We sample the structure for $S = 250$ times every $C = 15$ iterations. After learning the structure, we choose the best kernel parameters using the gradient approach mentioned above. We set the trade-off parameter in UCB to be $\beta(t) = 0.5 \log(2t)$, as suggested in (Rolland et al. 2018). For *discrete* experiments, we discretize each dimension to 50 levels, with the maximum number of individual acquisition function evaluations capped at 1000. For *continuous* experiments, we let each level’s grid size be $R = 4$ and the number of levels be $L = 4$ (see Fig. 2) with no maximum evaluation limits.

4.2 Metrics

Following (Wang et al. 2013), we plot the mean and $1/4$ standard deviation confidence intervals of the metrics over all

²Conditions include initial points, instances of the objective function, and random seeds used by the algorithm.

25 runs of the algorithm. For convenience, each plot’s legend is ordered according to the curves’ final y -value.

Graph Learning Performance. We measure how close the estimate G is from its target graph G_{opt} by calculating

$$F_1\text{score}(G) = 2 \frac{\text{Precision}(G) \times \text{Recall}(G)}{\text{Precision}(G) + \text{Recall}(G)}, \quad (8)$$

where $\text{Precision}(G) = \frac{|\text{Edges}(G) \cap \text{Edges}(G_{\text{opt}})|}{|\text{Edges}(G)|}$ and $\text{Recall}(G) = \frac{|\text{Edges}(G) \cap \text{Edges}(G_{\text{opt}})|}{|\text{Edges}(G_{\text{opt}})|}$, with $\text{Edges}(G)$ denoting the set of edges in graph G . A larger $F_1\text{score}$ indicates better graph learning performance.

Optimization Performance. In accordance with the ultimate goal of BO, we compute the *best regret* to measure closeness to the best value f_{\max} at iteration i :

$$R_t = f_{\max} - f_i^*, \quad (9)$$

where f_i^* denotes the best $f(x)$ value sampled up to iteration i . For functions where f_{\max} is unknown, we instead consider f_i^* , i.e., the *best value* found.

Discussion on Computation Time. In general, it is difficult to compare the amount of computational resources by various algorithms, as it is very much affected by many factors such as implementation, hardware, underlying GP backends, etc. However, we provide a brief discussion of the general trends observed. We generally found LineBO to be one of the faster approaches due to the use of 1D subroutines, though we also found its optimization perform to be limited in several cases. A fairly similar discussion applies to REMBO. On the other hand, the computational requirements of the *additive* methods are somewhat easier to compare in a fair manner, as we now discuss.

Cost Efficiency. For the additive methods, we compute the *Message Passing Cost* counting the number of individual acquisition function (ϕ^G) evaluations; see (S4) in the appendix. This metric is a proxy for the computational resources used in the optimization of the acquisition function. While it may not always correspond exactly to the total computation time, we expect that each message passing operation for Tree is *at least* as fast as in Graph No-Overlap and Graph Overlap. This is because Tree only works with functions containing only one or two variables, whereas the others may contain a larger number of variables.

4.3 Experiments with Additive GP Functions

We first compare Tree to other additive methods for functions drawn from a GP with additive structure. We focus our discussion on understanding the additive methods’ scaling ability and performance. Afterwards, we compare Tree to other methods using various non-GP functions. On all synthetic experiments, we add Gaussian $\mathcal{N}(0, 0.15^2)$ noise to simulate noise that occurs in real-world applications.

Similar to (Rolland et al. 2018), we test our algorithm on synthetic data by sampling functions from GPs with several different additive dependency structures. We use an RBF kernel with corresponding dimensional lengthscale and scale

parameters set to $\sigma_i^{\text{opt}} = 1$ and $l_i^{\text{opt}} = 0.2$ for all i . We tested several dependency structures; three notable examples are illustrated in Fig. 4, and a full list is given in the appendix.

In Fig. 3a, it is unsurprising that Tree outperforms the other additive methods for Star-25. The dependency graph of Star-25 is indeed a tree, enabling our method to be effective in learning the dependency structure. From Fig. S3e in the appendix, by plotting $F_1\text{score}$ over iterations, we observe that it is efficient in learning the dependency structure. The dependency structure learned by Tree is closest to the ground-truth throughout the experiment, when compared with other additive models. This efficiency is also reflected in Fig. S3f, where Tree achieves the best performance as a function of the message passing cost. We additionally demonstrate in the appendix that the reduction in cost becomes significantly higher in the case of continuous domains, achieving better performance return on cost than other additive methods.

Next, we turn to the case that the underlying graph is not a tree. Fig. 3b-3c corresponds to the Grid- 3×3 structure, and we find that Graph Overlap performs the best in terms of learning the dependency structure. This is because, for the grid graph model, only Graph Overlap’s underlying structural assumptions are correct. Both Tree and Graph No-Overlap face difficulty learning the graph accurately, albeit worse for Graph No-Overlap. Interestingly, Tree still remains competitive in terms of optimization performance despite poorer graph learning. That is, when Tree makes errant connections (or errant non-connections) in the dependency graph, the performance does not degrade significantly, and the algorithm can tweak other parameters (e.g., σ_i and l_i) to minimize the effect of any errant connections. From Fig. 3b, despite all additive algorithms being mutually competitive in terms of regret, both Graph No-Overlap and Graph Overlap needed more acquisition function evaluations to achieve the same performance as Tree (more than triple for Graph No-Overlap); see Fig. S4l in the appendix. In this instance, Graph No-Overlap’s pairwise disjoint assumption not only results in worse graph learning, but also worse cost efficiency. Next, we compare Graph No-Overlap and Tree using an Ancestry-132 dependency structure (132D).³ We found that Graph Overlap was unable to complete such high-dimensional experiments in a reasonable time. For Graph No-Overlap to work efficiently, we limited the maximum clique size, consider limits of both 5 and 10, represented by Graph No-Overlap (5) and Graph No-Overlap (10) respectively. In Fig. 3d-3e, we find Tree performing best in high-dimensions, and being the most cost efficient.

Scalability. Here, we test Tree’s scalability to higher dimensions up to 225D, focusing on studying how the total cumulative message passing cost incurred scales as dimension increases. We used the same setup and parameters as Sec. 4.3, across additive grid structures of varying sizes – Grid- $i \times i$ for $i \in [2, 15]$. We again include Graph No-Overlap (5) and Graph No-Overlap (10) for this experiment.

From Fig. 3f, we can see that the amount of cost needed for Graph Overlap and Graph No-Overlap quickly increases as

³See the appendix for more details on Ancestry-132.

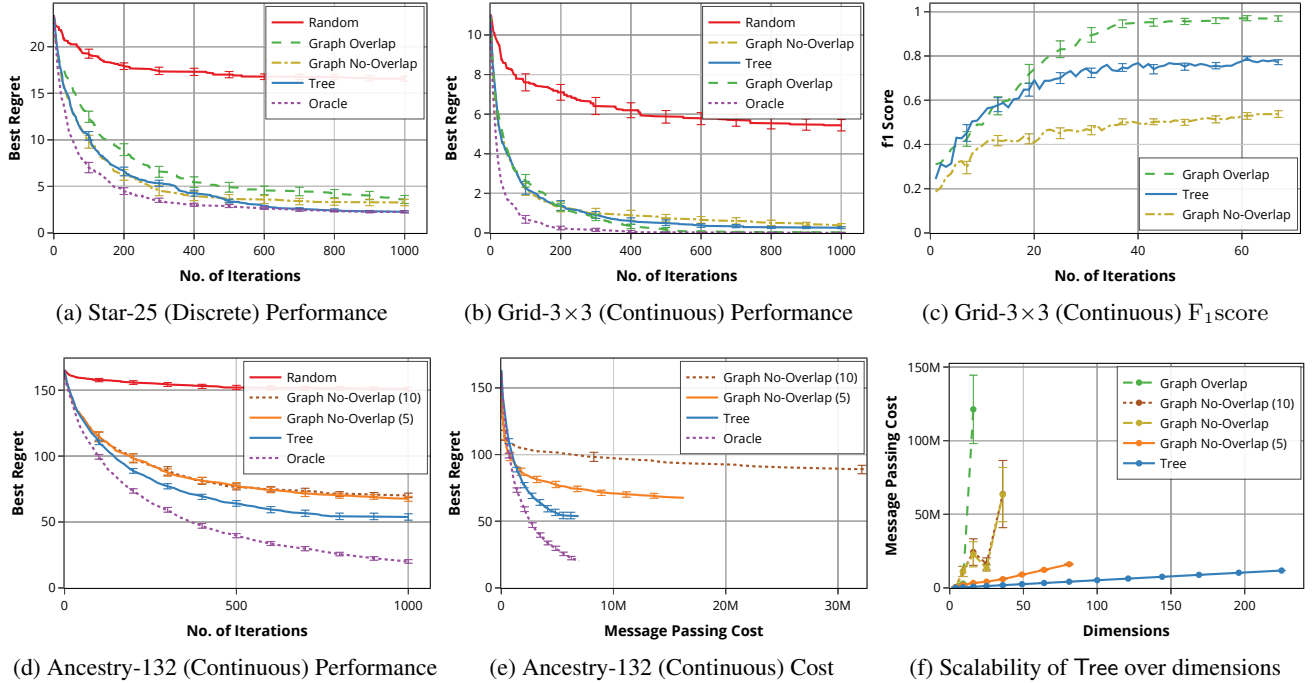


Figure 3: Summarized comparison of various additive methods across various functions.

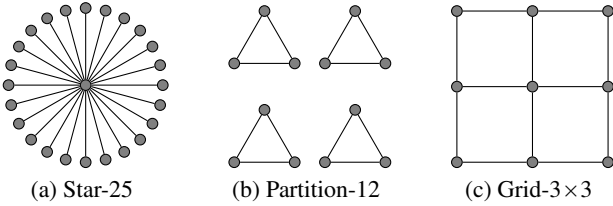


Figure 4: Synthetic Dependency Graphs Structures.

the dimensionality increases. In fact, we were unable to complete the experiment for larger grids in a reasonable amount of time. Recalling that Graph Overlap runs in time exponential in the size of the maximum clique of the triangulated dependency graph (Rolland et al. 2018), we note that even if that clique size does not grow large for the *true* graph, it may still tend to increase for the *estimated* graph. Similarly, Graph No-Overlap may be slow due to the consideration of large cliques, unless the clique size is explicitly limited. Even after imposing the limits, we found that Tree still incurs the lowest cost when compared with both Graph No-Overlap (5) and Graph No-Overlap (10). This is because, for tree structures, the message passing cost is quadratic in the number of discretization levels of a single dimension.

4.4 Experiments with Non-GP Functions

Non-GP Synthetic Functions. Here we test our algorithm against commonly used BO synthetic function benchmarks (Oh, Gavves, and Welling 2018; Kirschner et al. 2019), including Hartmann6 (6D) and Stybtang250 (250D). We also

tested Tree on benchmarks with invariant subspaces; following the setup in (Kirschner et al. 2019), Hartmann6+14Aux (20D) was obtained by augmenting the synthetic functions with 14 auxiliary dimensions. In Fig. 5a, we see that the regret of Tree reduces rapidly compared to other methods, with variants of LineBO catching up in later iterations. In Fig. 5b, we see that Tree again manages to scale well in higher-dimensional synthetic functions. From additional synthetic experiments (Fig. S6a-S6f in the appendix), Tree is also competitive against LineBO variants across both lower and higher dimensional settings, even in cases with invariant subspaces.

Linear Programming Solver. We consider tuning the parameters of *lpsolve*, an open-source Mixed Integer Linear Programming (MILP) solver (Berkelaar, Eikland, and Notebaert 2004). The parameters within each algorithm typically have some relationship with each other; tweaking a parameter can potentially affect another. We consider a similar configuration problem as defined by (Hutter, Hoos, and Leyton-Brown 2010; Wang et al. 2013), focusing on tuning *lpsolve*’s 74 parameters - 59 binary, 10 ordinal and 5 categorical. Our objective is to find the set of parameters of *lpsolve* that minimize the *optimality gap* it can achieve with a time limit of five seconds for the MIP encoding ‘misc05inf’ found in the benchmark MIPLIB (miplib2017 2018).

From Fig. 5c, we observe that REMBO is competitive in performance for optimizing the linear programming solver, as parameter optimization problems often have low effective dimensionality (Wang et al. 2013; Hoos and Leyton-Brown 2014). Despite being based on a very different notion of

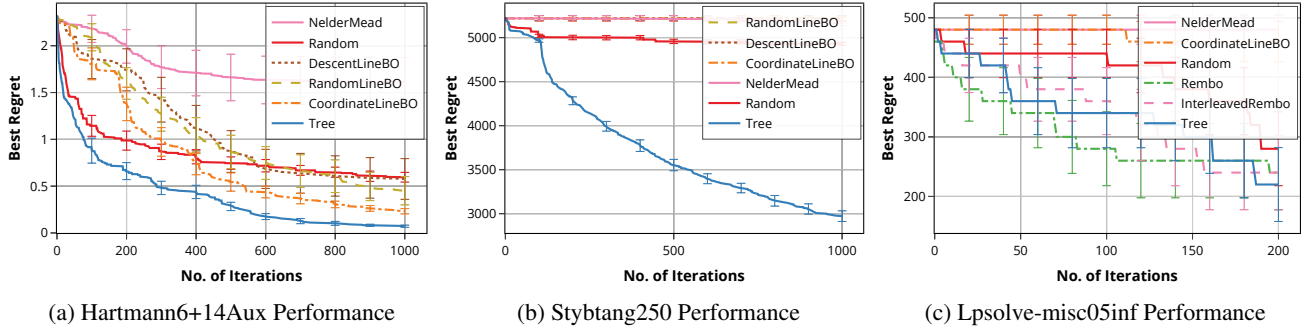


Figure 5: Comparison of various optimization algorithms for both synthetic functions and Lpsolve functions.

structure, Tree attains better performance than REMBO in this example, with both clearly outperforming Random. In the appendix, we provide two additional lpsolve examples in which Tree outperforms REMBO.

Additional Experiments. Additional experiments on the NAS-Bench-101 (NAS) dataset (Ying et al. 2019; Klein and Hutter 2019) and BO-based adversarial attacks (BA) (Ru et al. 2020) can be found in the appendix.

5 Conclusion

For the problem of GP optimization with generalized additive models, we traded off expressivity for computational efficiency and ease of model learning by reducing the model complexity, constraining the dependency graph to tree structures. Our method efficiently learns the additive tree structure using Gibbs Sampling and edge mutation, suitable for resource-limited settings in line with the primary motivation of BO. Besides, we presented a zooming-based message passing approach that can benefit BO with generalized additive models in continuous domains, with or without tree structures. We demonstrated that Tree is competitive on both synthetic functions and real datasets, and that the computation can be significantly reduced compared to more complex graph structures, without sacrificing the optimization performance.

Acknowledgments

This work was supported by both the Singapore National Research Foundation (NRF) under grant number R-252-000-A74-281 and the AWS Cloud Credits for Research program.

References

- Auer, P. 2002. Using confidence bounds for exploitation-exploration trade-offs. *Journal of Machine Learning Research* 3(Nov):397–422.
- Berkelaar, M.; Eikland, K.; and Notebaert, P. 2004. *lp solve 5.5*, open source (mixed-integer) linear programming system. Software.
- Chen, B.; Castro, R. M.; and Krause, A. 2012. Joint optimization and variable selection of high-dimensional Gaussian processes. In *Int. Conf. Mach. Learn. (ICML)*, 1379–1386.
- Cormen, T. H.; Leiserson, C. E.; Rivest, R. L.; and Stein, C. 2009. *Introduction to algorithms*. MIT press.
- Cui, J.; Yang, B.; and Hu, X. 2019. Deep Bayesian optimization on attributed graphs. In *AAAI Conf. on Art. Intel.*, volume 33, 1377–1384.
- Djolonga, J.; Krause, A.; and Cevher, V. 2013. High-dimensional Gaussian process bandits. In *Conf. Neur. Inf. Proc. Sys. (NIPS)*, 1025–1033.
- Eriksson, D.; Pearce, M.; Gardner, J.; Turner, R. D.; and Poloczek, M. 2019. Scalable Global Optimization via Local Bayesian Optimization. In Wallach, H.; Larochelle, H.; Beygelzimer, A.; d’Alché-Buc, F.; Fox, E.; and Garnett, R., eds., *Advances in Neural Information Processing Systems*, volume 32, 5496–5507. Curran Associates, Inc.
- Frazier, P. I. 2018. A tutorial on Bayesian optimization. *arXiv preprint arXiv:1807.02811*.
- Gonzalez, J.; Lezmi, E.; Roncalli, T.; and Xu, J. 2019. Financial applications of Gaussian processes and Bayesian optimization. *arXiv preprint arXiv:1903.04841*.
- Hoang, T. N.; Hoang, Q. M.; Ouyang, R.; and Low, K. H. 2018. Decentralized high-dimensional Bayesian optimization with factor graphs. In *AAAI Conf. on Art. Intel.*
- Hoos, H., and Leyton-Brown, K. 2014. An efficient approach for assessing hyperparameter importance. In *Int. Conf. Mach. Learn. (ICML)*, 754–762.
- Hutter, F.; Hoos, H. H.; and Leyton-Brown, K. 2010. Automated configuration of mixed integer programming solvers. In *Int. Conf. on Integration of AI and OR Techniques in Constraint Programming for Combinatorial Optimization Problems (CPAIOR)*, 186–202. Springer.
- Jaquier, N.; Rozo, L.; Calinon, S.; and Bürger, M. 2020. Bayesian Optimization meets Riemannian Manifolds in Robot Learning. In *Conference on Robot Learning*, 233–246. PMLR.
- Jenatton, R.; Archambeau, C.; González, J.; and Seeger, M. 2017. Bayesian optimization with tree-structured dependencies. In *Int. Conf. Mach. Learn. (ICML)*.
- Kandasamy, K.; Schneider, J.; and Póczos, B. 2015. High dimensional Bayesian optimisation and bandits via additive models. In *Int. Conf. Mach. Learn. (ICML)*, 295–304.
- Kirschner, J.; Mutny, M.; Hiller, N.; Ischebeck, R.; and Krause, A. 2019. Adaptive and safe Bayesian optimization in high dimensions via one-dimensional subspaces. In *Int. Conf. Mach. Learn. (ICML)*, 3429–3438.
- Klein, A., and Hutter, F. 2019. Tabular benchmarks for joint architecture and hyperparameter optimization. *arXiv preprint arXiv:1905.04970*.

- Li, C.-L.; Kandasamy, K.; Póczos, B.; and Schneider, J. 2016. High dimensional Bayesian optimization via restricted projection pursuit models. In *Int. Conf. Art. Intel. Stats. (AISTATS)*, 884–892.
- Li, C.; Gupta, S.; Rana, S.; Nguyen, V.; Venkatesh, S.; and Shilton, A. 2017. High dimensional Bayesian optimization using dropout. In *Int. Joint Conf. on Art. Intel. (IJCAI)*, 2096–2102.
- Lu, X.; Gonzalez, J.; Dai, Z.; and Lawrence, N. 2018. Structured variationally auto-encoded optimization. In *Int. Conf. Mach. Learn. (ICML)*, 3267–3275.
- Ma, X., and Blaschko, M. 2020. Additive Tree-Structured Covariance Function for Conditional Parameter Spaces in Bayesian Optimization. *Int. Conf. Art. Intel. Stats. (AISTATS)*.
2018. MIPLIB 2017. <http://miplib.zib.de>.
- Moćkus, J. 1975. On Bayesian methods for seeking the extremum. In *Optimization Techniques IFIP Technical Conf.*, 400–404. Springer.
- Moriconi, R.; Kumar, K.; and Deisenroth, M. P. 2019. High-dimensional bayesian optimization with manifold gaussian processes. *arXiv preprint arXiv:1902.10675*.
- Murphy, K. P. 2012. *Machine learning: A probabilistic perspective*. MIT press.
- Mutny, M., and Krause, A. 2018. Efficient High Dimensional Bayesian Optimization with Additivity and Quadrature Fourier Features. In Bengio, S.; Wallach, H.; Larochelle, H.; Grauman, K.; Cesa-Bianchi, N.; and Garnett, R., eds., *Advances in Neural Information Processing Systems*, volume 31, 9005–9016. Curran Associates, Inc.
- Nayebi, A.; Munteanu, A.; and Poloczek, M. 2019. A framework for Bayesian optimization in embedded subspaces. In *Int. Conf. Mach. Learn. (ICML)*, 4752–4761.
- Oh, C.; Gavves, E.; and Welling, M. 2018. BOCK: Bayesian optimization with cylindrical kernels. In *Int. Conf. Mach. Learn. (ICML)*, 3868–3877.
- Rolland, P.; Scarlett, J.; Bogunovic, I.; and Cevher, V. 2018. High-dimensional Bayesian optimization via additive models with overlapping groups. In *Int. Conf. Art. Intel. Stats. (AISTATS)*, 298–307.
- Ru, B.; Cobb, A.; Blaas, A.; and Gal, Y. 2020. BayesOpt Adversarial Attack. In *Proc. of the International Conference on Learning Representations*.
- Sano, S.; Kadowaki, T.; Tsuda, K.; and Kimura, S. 2019. Application of Bayesian optimization for pharmaceutical product development. *Journal of Pharmaceutical Innovation* 1–11.
- Sedgewick, R., and Wayne, K. 2011. *Algorithms*. Addison-wesley professional.
- Snoek, J.; Rippel, O.; Swersky, K.; Kiros, R.; Satish, N.; Sundaram, N.; Patwary, M.; Prabhat, M.; and Adams, R. 2015. Scalable Bayesian optimization using deep neural networks. In *Int. Conf. Mach. Learn. (ICML)*, 2171–2180.
- Snoek, J.; Larochelle, H.; and Adams, R. P. 2012. Practical Bayesian optimization of machine learning algorithms. In *Conf. Neur. Inf. Proc. Sys. (NIPS)*, 2951–2959.
- Spruyt, V. 2014. The curse of dimensionality in classification. *Computer Vision for Dummies* 21(3):35–40.
- Srinivas, N.; Krause, A.; Kakade, S.; and Seeger, M. 2010. Gaussian process optimization in the bandit setting: No regret and experimental design. In *Int. Conf. Mach. Learn. (ICML)*, 1015–1022.
- Swersky, K.; Snoek, J.; and Adams, R. P. 2013. Multi-task Bayesian optimization. In *Conf. Neur. Inf. Proc. Sys. (NIPS)*, 2004–2012.
- Wang, Z.; Zoghi, M.; Hutter, F.; Matheson, D.; and De Freitas, N. 2013. Bayesian optimization in high dimensions via random embeddings. In *Int. Joint Conf. on Art. Intel. (IJCAI)*.
- Wang, Z.; Li, C.; Jegelka, S.; and Kohli, P. 2017. Batched high-dimensional Bayesian optimization via structural kernel learning. In *Int. Conf. Mach. Learn. (ICML)*, 3656–3664. JMLR. org.
- Wang, Z.; Gehring, C.; Kohli, P.; and Jegelka, S. 2018. Batched large-scale Bayesian optimization in high-dimensional spaces. In *Int. Conf. Art. Intel. Stats. (AISTATS)*, 745–754.
- Wang, Z. 2016. *Practical and theoretical advances in Bayesian optimization*. Ph.D. Dissertation, University of Oxford.
- Ying, C.; Klein, A.; Christiansen, E.; Real, E.; Murphy, K.; and Hutter, F. 2019. NAS-Bench-101: Towards reproducible neural architecture search. In *Int. Conf. Mach. Learn. (ICML)*, 7105–7114.
- Yogatama, D.; Kong, L.; and Smith, N. A. 2015. Bayesian optimization of text representations. In *Conf. on Empirical Methods in NLP (EMNLP)*, 2100–2105.
- Zhang, M.; Li, H.; and Su, S. 2019. High Dimensional Bayesian Optimization via Supervised Dimension Reduction. In *Proceedings of the Twenty-Eighth International Joint Conference on Artificial Intelligence, IJCAI-19*, 4292–4298. International Joint Conferences on Artificial Intelligence Organization.

Supplementary Document (Appendix): High-Dimensional Bayesian Optimization via Tree-Structured Additive Models

AAAI 2021

Eric Han,¹ Ishank Arora,² Jonathan Scarlett^{1,3}

¹School of Computing, National University of Singapore

²Indian Institute of Technology (BHU) Varanasi

³Department of Mathematics & Institute of Data Science, National University of Singapore
eric_han@nus.edu.sg, ishank.arora.cse14@iitbhu.ac.in, scarlett@comp.nus.edu.sg

S1 Learning the Kernel Parameters

We consider selecting the kernel parameters by maximizing the marginal likelihood, and specifically adopt a well-established gradient approach. To implement gradient-based methods, we compute the partial derivatives of the log-likelihood with respect to the dimensional hyperparameters $\Theta = \{\theta_i : (\ell_i, \sigma_i)\}_{i=1}^D$ as (Williams and Rasmussen 2006):

$$\frac{\partial}{\partial \theta} \rho(Z, \theta) = \frac{1}{2} \text{Tr} \left[(\alpha \alpha^T - K^{-1}) \sum_{G \in \mathcal{G}} \left(\frac{\partial \kappa^G}{\partial \theta} \right) \right]. \quad (\text{S1})$$

The inner partial derivative $\partial \kappa^G / \partial \theta$ depends on the choice of kernel. The partial derivative with respect to each lengthscale ℓ_i can be computed directly, and for the kernels we consider, this is facilitated by the availability of closed-form kernel expressions. Following our definition of the scale parameter $\sigma^G = \sqrt{\sum_{i \in G} \sigma_i^2}$, the partial derivative with respect to each dimensional scale parameter σ_j is

$$\frac{\partial \kappa^G}{\partial \sigma_j} = \frac{\partial \kappa^G}{\partial \sigma^G} \left(\frac{\partial}{\partial \sigma_j} \sqrt{\sum_{i \in G} \sigma_i^2} \right) = \frac{\partial \kappa^G}{\partial \sigma^G} \times \frac{\sigma_j}{\sigma^G}. \quad (\text{S2})$$

Again, $\partial \kappa^G / \partial \sigma^G$ is computed directly from the closed-form kernel expression. Following common practice (Pedregosa et al. 2011; GPy since 2012), we restrict the optimization of the dimensional parameters to $\ell_j \in [10^{-2}, 10^5]$ and $\sigma_j \in [\sqrt{0.1}, 10^5]$, ensuring that the kernel parameters are positive and avoid extreme values that can lead to numerical issues. In addition, we avoid making the lower bound on each σ_j too small, accounting for the equivalent effect in the graph learning of not creating an edge between two variables. There exist several gradient-based optimization techniques that can be used, e.g., Limited-Memory Broyden-Fletcher-Goldfarb-Shanno Algorithm (L-BFGS), Truncated Newton algorithm (TNC), and others. We adopt TNC for all experiments except BO-based adversarial attacks, in which we use L-BFGS for consistency with a previous baseline. In addition, we impose limits on the maximum number of function evaluations in

terms of the iteration index t according to the following:

$$m(t) = M_0 \exp \left(\frac{\log(M_{N_{iter}})}{N_{iter}} \times t \right). \quad (\text{S3})$$

We found that by increasing the maximum number of function evaluations over iterations, we can get a good trade-off between exploration and exploitation, avoiding overfitting of kernel parameters. In (S3), we set $M_0 = 1$ and $M_{N_{iter}} = 2D$.

S2 Maximization over Discrete Domains

For BO to be effective in high dimensions, the underlying acquisition function needs to be optimized efficiently. In Alg. S1, we present a simplified variant of the algorithm proposed by (Rolland et al. 2018) for generalized additive models. We deal with the optimization of the acquisition function of a given dependency structure \mathcal{G} and discrete domain $\mathcal{X} = \times_{i=1}^D \mathcal{X}_i$ with $\mathcal{X}_i = [[a_i, b_i]]$, discretized uniformly with R discrete values between a_i and b_i inclusive. The algorithm uses the message passing technique on a triangulated graph, similar to the efficient maximization of probability in Markov random fields (Wainwright 2015). We will shortly discuss a simplified variant in the case of tree-structured graphs.

Alg. S1 makes use of a junction tree, with each node in the junction tree representing a maximal clique of the triangulated dependency graph. Since we have changed the structure of the dependency graph by triangulation, we need to carefully account for the individual acquisition functions ϕ^G (see 4), as they are no longer directly equivalent to the function that we are optimizing on each node of the junction tree. We simplify Rolland *et al.*'s method by excluding the acquisition functions ϕ^G that have been previously maximized:

$$\psi^C(x^C) = \sum_{\forall G \in \mathcal{G}: (\phi^G \notin \Phi \wedge G \subseteq C)} \phi^G(x^G), \quad (\text{S4})$$

where Φ denotes the set of acquisition functions that have been previously maximized. Fig. S1 shows an example.

Complexity. Alg. S1 applies to arbitrary graph structures, allowing this technique to be applied to general additive models. The complexity of running the algorithm is exponential in the size of the maximum clique of the triangulated

Algorithm S1: MSG-PASSING-DISCRETE

```

1 Select a node  $R$  to root the junction tree
2  $D_{\text{tree}} \leftarrow$  depth of the rooted tree
3 Initialize  $\Phi \leftarrow \emptyset$ 
4 for  $d = D_{\text{tree}}, \dots, 1$  do
5   for every node  $C$  at distance  $d$  from  $R$  do
6      $C_p = \text{parent}(C)$ 
7     Common variables  $I \leftarrow C \cap C_p$ 
8     Marginal variables  $J \leftarrow C \setminus C_p$ 
9     for  $x^I \in \mathcal{X}^I$  do
10       $M_{C \rightarrow C_p}[x^I] =$ 
11         $\max_{x^J \in \mathcal{X}^J} \psi^C(x^I, x^J) +$ 
12         $\sum_{C_c \in \text{children}(C)} M_{C_c \rightarrow C}[x^{C \cap C_c}]$ 
13      Update  $\Phi$  to include all  $\phi^G$  that were
14      optimized in  $\psi^C$ 
15 return  $\max_{x^R \in \mathcal{X}^R} \psi^R(x^R) +$ 
16  $\sum_{C_c \in \text{children}(R)} M_{C_c \rightarrow R}[x^{R \cap C_c}]$ 

```

graph (Rolland et al. 2018). Hence, the algorithm can benefit from choosing a triangulation that minimizes the size of the maximal clique (Arnborg, Corneil, and Proskurowski 1987; Cano and Moral 1994). In Tree, the dependency structure is a tree. As a result, there are no cycles, and there is no need to triangulate the tree \mathcal{G} . Moreover, the function of ψ^C can be simplified to $\psi^C = \phi^C$. Hence, the complexity of the maximization is reduced to quadratic in R .

S3 Implementation Details

We implemented all algorithms in Python 3.8.3. The Python environments are managed using Conda, and experiments are managed using MLflow (Zaharia et al. 2018). The specific hardware used is not crucial, as we ensure consistent runs across different hardware via the use of Conda and MLflow.

Both Graph Overlap and Graph No-Overlap are reimplemented using the original implementations and the details from their publications (Rolland et al. 2018; Kandasamy, Schneider, and Póczos 2015).

For LineBO algorithms, we use the original author’s implementation.¹ The REMBO and InterleavedREMBO implementations are also based on the implementation found in LineBO’s repository. We additionally consider the heuristic NelderMead algorithm (Nelder and Mead 1965), which is provided by SciPy, as in LineBO’s repository. Implementation of the algorithms used in the BO-Based Adversarial Attack experiments are from the original author’s repository.²

S4 Further Experimental Details and Results

The existing algorithms that we use in our experiments, along with their parameters, are summarized in Table S1. We note that for parameters unique to LineBO, we have used the recommended parameters as stated in (Kirschner et al. 2019),

¹<https://github.com/jkirschner42/LineBO>

²https://github.com/rubinxin/BayesOpt_Attack

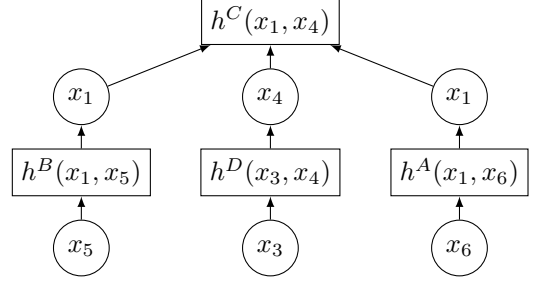


Figure S1: Illustration of the optimization of the acquisition function on the graph \mathcal{G} shown in Fig. 1. First, the leaves of the junction tree perform partial maximization of the functions f^B , f^D , and f^A over their respective variables x_4 , x_2 and x_5 . The result of the partial maximization is a ‘conditional’ maximization over the other variables. These ‘conditional’ maximizations are passed as messages to the nodes above. In this manner, the messages are passed until the root node, and the correct answer is returned.

Method	Unique parameter values
DescentLineBO	As per hartmann6.yaml ³
RandomLineBO	
CoordinateLineBO	
REMBO	Embedded Dimension = \sqrt{D}
InterleavedREMBO	Interleaved Runs = 4
NelderMead	Contraction Factor = 0.3
	Initial Stepsize = 0.1
	Restart Threshold = 0.001
Graph No-Overlap	Max Clique Size = D
Graph Overlap	N/A
ADDGP-BO	As per defaults in repository ²
GP-BO	

Table S1: State-of-the-art methods’ parameters values

Type	Name	Dim.	No. of Exps.
Add. GP Fns.	Grid-3×3	9	250
	Star-10	10	250
	Partition-12	12	250
	Star-25	25	250
	Ancestry-132	132	125
Add. GP Fns. (Scalability)	Grid-2×2	4	125
	Grid-3×3	9	125
	Grid-4×4	16	125
	Grid-5×5	25	100
	Grid-6×6	36	100
	Grid-7×7	49	50
	Grid-8×8	64	50
	Grid-9×9	81	50
	Grid-10×10	100	25
	Grid-11×11	121	25
	Grid-12×12	144	25
	Grid-13×13	169	25
	Grid-14×14	196	25
	Grid-15×15	225	25
Non-GP Fns.	Camelback2	2	150
	Hartmann6	6	150
	Camelback2+10Aux	12	150
	Hartmann6+14Aux	20	150
	Rosenbrock20	20	150
	Stybtang250	250	150
NAS	naval	9	100
	parkinsons		100
	protein		100
	slice		100
BA Lpsolve	misc05inf	74	150
	mttest4ma		150
	qiu		150
BA	MNIST	196	1800

Table S2: Summary of both Synthetic (top) and Real (bottom) functions used in our experiments; by type, dimensionality.

specifically the parameters found in their Hartmann6 experiments.³

A summary of the functions that were used in our experiments is given in Table S2. We ran the functions in the ‘Additive GP Functions’ experiments over both continuous and discrete domains, investigating Tree’s performance. The rest of the functions were run over continuous domains.

S4.1 Additive GP Functions

In addition to the observations made in the main document, Tree’s efficiency is also demonstrated for both discrete and continuous functions – see Fig. S3-S4. We see that Tree is able to learn a tree structure that performs well while being cost-efficient, even when the hypothesis that Tree considers

³In the repository of (Kirschner et al. 2019) – <https://github.com/jkirschner42/LineBO/blob/master/config/hartmann6.yaml>

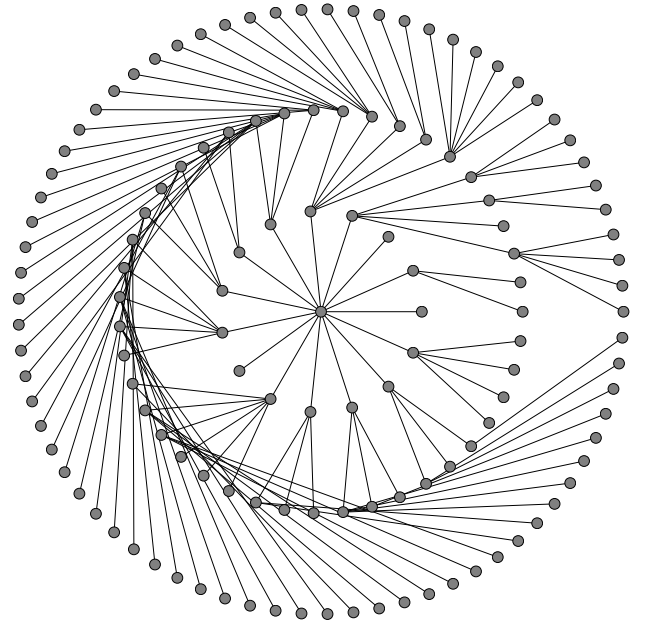


Figure S2: Ancestry-132 Dependency Graph Structure.

is not realizable in both Grid-3×3 and Partition-12. In the case of Partition-12, Tree’s graph learning is not realizable, whereas both Graph No-Overlap and Graph Overlap are realizable. The results for Partition-12 lends further support to the discussion in Sec. 4.3 on Grid-3×3, Tree remains competitive in terms of the optimization performance despite poorer graph learning. Most surprisingly, Tree is sometimes able to outperform Oracle; see Fig. S3g and Fig. S3j. To understand this, recall from Sec. 4.1 that we limited the number of individual acquisition function evaluations to 1000. For tree structures, we are dealing with functions of at most two variables, whereas this limitation in evaluations has the greatest impact on graphs whose triangulated versions have larger cliques. In the present example, the true graph provided for Oracle contains cliques of size at least 3 after triangulation. These results suggest that even when the hypothesis is not realizable, the performance penalty for Tree is minor. That is, the lack of model richness is compensated for by faster model selection and the ability to optimize the acquisition function accurately.

In addition, we ran experiments on Ancestry-132, a 132-dimensional family tree of (Nicolas Kruchten 2015), shown in Fig. S2. The graph was obtained from the original author’s repository and converted to an equivalent representation for use in our codebase.⁴ We used the graph structure in the same way as any of the synthetic dependency graphs structures, which we specified in Sec. 4.3. We note that for higher dimensions, F_1 score in Fig. S5b may potentially improve by increasing the number of graphs S sampled in Alg. 3;

⁴<https://raw.githubusercontent.com/nicolaskruchten/genealogy/master/family.json>

we have adopted the same choice across all experiments for consistency.

S4.2 Non-GP Functions

Synthetic Functions. Camelback2 is a commonly used BO benchmark function with two dimensions that has two global minima with the same value of -1.0316 (Eggenberger et al. 2013). Hartmann6 (6D) is defined as

$$f(x) = - \sum_{i=1}^4 \alpha_i \exp \left(- \sum_{j=1}^6 A_{ij} (x_j - P_{ij})^2 \right), \quad (\text{S5})$$

and has seven minima – six local and one global (Eggenberger et al. 2013). We use implementations from HPOLib2, letting α , A and P be as defined in (Eggenberger et al. 2013). Rosenbrock20 (20D) is a synthetic function that have a single global optima at $x = (1.0, \dots, 1.0)$ with value of 0. Rosenbrock20 is challenging to optimize, as the values returned by the function have a wide range even when using a small domain of $[0, 1]$. The Styblinski-Tang function, Stybtang250 (250D):

$$f(x) = \frac{1}{2} \sum_{i=1}^{250} (x_i^4 - 16x_i^2 + 5x_i), \quad (\text{S6})$$

has a global minimum of approximately -39.16599×250 at $x = (-2.9, \dots, -2.9)$. We restrict the domain of the function to $[-4, 4]^{250}$. Similar to Rosenbrock20, the values returned by Stybtang250 has a wide range.

From Fig. S6a-S6f, we observe that Tree consistently performs well across these synthetic functions. In contrast, the LineBO algorithms perform better on certain functions than others, and can face certain limitations. For instance, from Fig. S6e, we see that LineBO algorithms can incur higher regret to perform when the range of the function is large, which applies to both Rosenbrock20 and Stybtang250.

Linear Programming Solver. Here, we include further lpsolve experiments to supplement those in the main text. REMBO and its interleaved variant are effective in some cases (e.g., Fig. S7a), but are slow to converge in others (e.g., Fig. S7a, Fig. S7b). In contrast, Tree performs well across all three datasets.

NAS Benchmarks. We run experiments on the NAS-Bench-101 (NAS) dataset (Ying et al. 2019; Klein and Hutter 2019). This dataset serves as a convenient hyperparameter benchmark that allows us to quickly run hyperparameter optimization over a fully connected neural network. Traditionally, when we run hyperparameter optimization over a neural network, it would be slow, as training and testing a neural network would take substantial time. This benchmark pre-computes the results for all possible 62208 configurations (from 9 hyperparameters) defined in (Ying et al. 2019; Klein and Hutter 2019). Consequently, we have access to f_{\max} . We ran the experiments as described in (Klein and Hutter 2019), across all four NAS benchmarks (see Table S2).

The results from the NAS benchmarks suggest that most functions in this dataset have little additive structure. We

can observe this from the lack of significant difference between the graph-based algorithms across the NAS-naval, NAS-parkinsons and NAS-slice as shown in Fig. S8. There is a small performance edge that Tree achieves over the other algorithms in NAS-protein shown in Fig. S8c. The performance edge is gained efficiently, requiring lower cost when compared with the rest of the algorithms. Overall, these experiments suggest that Tree does not break down in datasets with little or no additive structure while retaining efficiency.

BO-Based Adversarial Attack. BO has recently been applied to *targeted* adversarial black-box attacks on neural networks. In particular, (Ru et al. 2020) proposed an approach based on the non-overlapping additive model from (Kandasamy, Schneider, and Póczos 2015). Their method achieves comparable success rates with fewer queries than certain state-of-the-art black-box attack methods for attacks on convolutional neural network (CNN) models. We adopt the same black-box function as (Ru et al. 2020), in which the input is an image perturbation and the output is the classification accuracy.

In this experiment, we adapt Tree in an analogous manner to (Ru et al. 2020) in order to perform adversarial black-box attacks on the CNN models. To maintain a fair comparison, we adopted the same experimental choices and parameters as (Ru et al. 2020) wherever possible, in particular using the Matérn- $5/2$ kernel, applying L-BFGS for kernel parameter optimization, performing graph and parameter learning according to the same regularly-spaced intervals (length 40 and 5 respectively), and using $N_{\text{init}} = 50$ initial random points.

The CNN models that we attack are also the same as (Tu et al. 2019; Alzantot et al. 2019; Ru et al. 2020). The image classifiers for the dataset MNIST (99.5% Accuracy) is taken from the author’s repository. Using the same reduction technique and dimensionality as (Ru et al. 2020; Tu et al. 2019), we perform the search on a reduced image dimension of $14 \times 14 \times 1$ for MNIST (196D). For the attack, we randomly select 50 correctly-classified images; then, for each image, we perform the attack for all target labels except the true label. We record the Attack Success Rate (ASR) (i.e., the proportion of times the attack succeeds in making the classifier output the target label, averaged across 450 runs) against the number of iterations. We used process time from Python’s standard library⁵, recording the total of both system and user process-wide CPU time. Considering that we executed the experiments over a heterogeneous cluster (randomly distributed) and other experimental considerations, this metric allows us to glean a rough measure of the algorithm’s efficiency.

We compare Tree to the implementations available in (Ru et al. 2020)’s repository. We note that the additive BO implementation (ADDGP-BO) is different from our implementation of Graph No-Overlap. In particular, they select the graph according the highest likelihood among a number of randomly-generated graphs, whereas we adopt the Gibbs sampling approach of (Wang et al. 2017; Rolland et al. 2018).

We focus on comparing against ADDGP-BO, as it was the

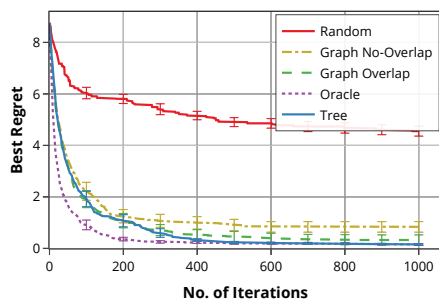
⁵https://docs.python.org/3/library/time.html#time.process_time

best overall method reported in (Ru et al. 2020). The results are presented in Fig. S9.⁶ We see in Fig. S9a that Tree is able to attack MNIST (196D) CNN model with a comparable success rate as ADDGP-BO, but with significantly reduced process time. The process time is lowest for GP-BO (an GP-UCB based baseline without additive structure, available in the repository of (Ru et al. 2020)), but at the cost of a significantly worse ASR.

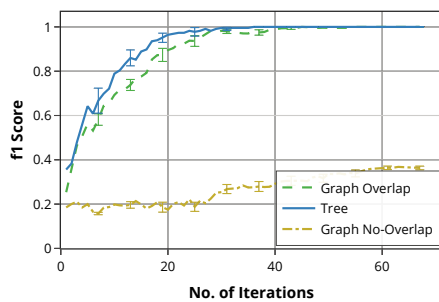
References (Appendix only)

- Alzantot, M.; Sharma, Y.; Chakraborty, S.; Zhang, H.; Hsieh, C.-J.; and Srivastava, M. B. 2019. Genattack: Practical black-box attacks with gradient-free optimization. In *Proceedings of the Genetic and Evolutionary Computation Conference*, 1111–1119.
- Arnborg, S.; Corneil, D. G.; and Proskurowski, A. 1987. Complexity of finding embeddings in a k -tree. *SIAM Journal on Algebraic Discrete Methods* 8(2):277–284.
- Cano, A., and Moral, S. 1994. Heuristic algorithms for the triangulation of graphs. In *International Conference on Information Processing and Management of Uncertainty in Knowledge-Based Systems*, 98–107. Springer.
- Eggersperger, K.; Feurer, M.; Hutter, F.; Bergstra, J.; Snoek, J.; Hoos, H.; and Leyton-Brown, K. 2013. Towards an empirical foundation for assessing Bayesian optimization of hyperparameters. In *NIPS Workshop on Bayesian Optimization in Theory and Practice*.
- GPY. since 2012. GPY: A Gaussian process framework in python. <http://github.com/SheffieldML/GPY>.
- Kandasamy, K.; Schneider, J.; and Póczos, B. 2015. High dimensional Bayesian optimisation and bandits via additive models. In *Int. Conf. Mach. Learn. (ICML)*, 295–304.
- Kirschner, J.; Mutny, M.; Hiller, N.; Ischebeck, R.; and Krause, A. 2019. Adaptive and safe Bayesian optimization in high dimensions via one-dimensional subspaces. In *Int. Conf. Mach. Learn. (ICML)*, 3429–3438.
- Klein, A., and Hutter, F. 2019. Tabular benchmarks for joint architecture and hyperparameter optimization. *arXiv preprint arXiv:1905.04970*.
- Nelder, J. A., and Mead, R. 1965. A simplex method for function minimization. *The Computer Journal* 7(4):308–313.
- Nicolas Kruchten. 2015. Visualizing Family Trees. <http://nicolas.kruchten.com/content/2015/08/family-trees/>. Accessed: 2020-06-01.
- Pedregosa, F.; Varoquaux, G.; Gramfort, A.; Michel, V.; Thirion, B.; Grisel, O.; Blondel, M.; Prettenhofer, P.; Weiss, R.; Dubourg, V.; Vanderplas, J.; Passos, A.; Cournapeau, D.; Brucher, M.; Perrot, M.; and Duchesnay, E. 2011. Scikit-learn: Machine learning in Python. *Journal of Machine Learning Research* 12:2825–2830.
- Rolland, P.; Scarlett, J.; Bogunovic, I.; and Cevher, V. 2018. High-dimensional Bayesian optimization via additive models with overlapping groups. In *Int. Conf. Art. Intel. Stats. (AISTATS)*, 298–307.
- Ru, B.; Cobb, A.; Blaas, A.; and Gal, Y. 2020. BayesOpt Adversarial Attack. In *Proc. of the International Conference on Learning Representations*.
- Tu, C.-C.; Ting, P.; Chen, P.-Y.; Liu, S.; Zhang, H.; Yi, J.; Hsieh, C.-J.; and Cheng, S.-M. 2019. Autozoom: Autoencoder-based zeroth order optimization method for attacking black-box neural networks. In *AAAI Conf. on Art. Intel.*, volume 33, 742–749.
- Wainwright, M. J. 2015. Graphical models and message-passing algorithms: Some introductory lectures. In *Mathematical Foundations of Complex Networked Information Systems*. Springer. 51–108.
- Wang, Z.; Li, C.; Jegelka, S.; and Kohli, P. 2017. Batched high-dimensional Bayesian optimization via structural kernel learning. In *Int. Conf. Mach. Learn. (ICML)*, 3656–3664. JMLR. org.
- Williams, C. K., and Rasmussen, C. E. 2006. *Gaussian processes for machine learning*, volume 2. MIT press Cambridge, MA.
- Ying, C.; Klein, A.; Christiansen, E.; Real, E.; Murphy, K.; and Hutter, F. 2019. NAS-Bench-101: Towards reproducible neural architecture search. In *Int. Conf. Mach. Learn. (ICML)*, 7105–7114.
- Zaharia, M.; Chen, A.; Davidson, A.; Ghodsi, A.; Hong, S. A.; Konwinski, A.; Murching, S.; Nykodym, T.; Ogilvie, P.; Parkhe, M.; et al. 2018. Accelerating the Machine Learning Lifecycle with MLflow. *IEEE Data Eng. Bull.* 41(4):39–45.

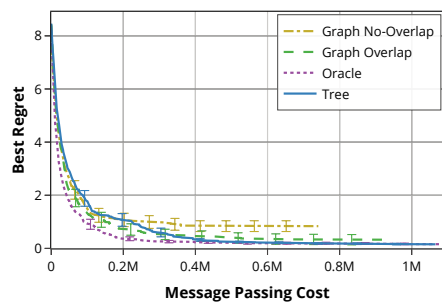
⁶Attacks that took at least three times longer than 99% of the runs were marked as unsuccessful.



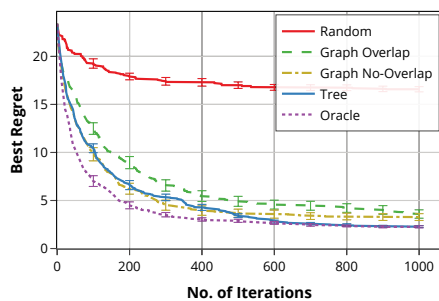
(a) Star-10 (Discrete) Performance



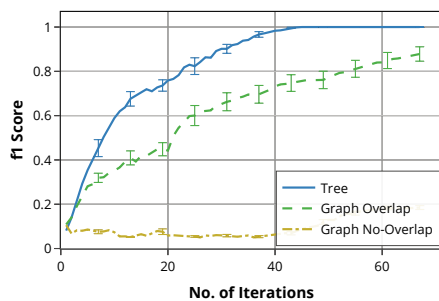
(b) Star-10 (Discrete) F₁score



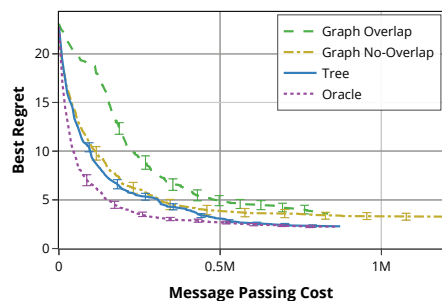
(c) Star-10 (Discrete) Cost



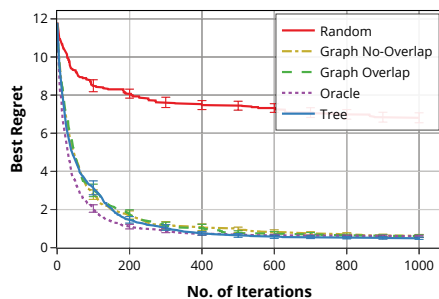
(d) Star-25 (Discrete) Performance



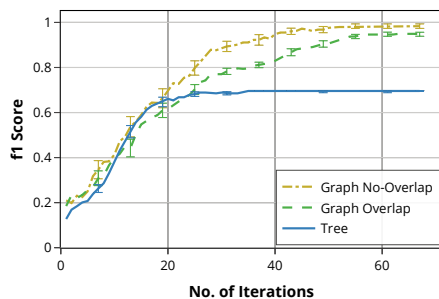
(e) Star-25 (Discrete) F₁score



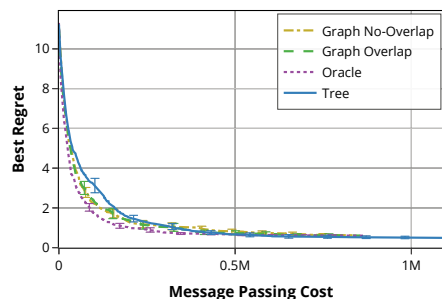
(f) Star-25 (Discrete) Cost



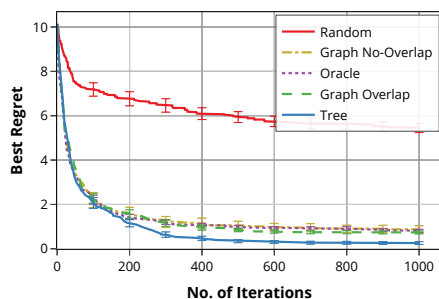
(g) Partition-12 (Discrete) Performance



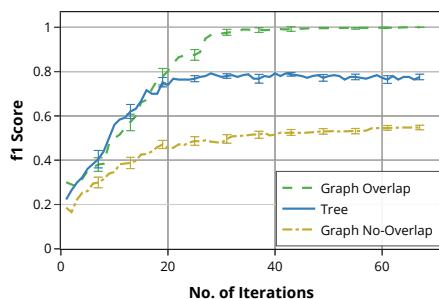
(h) Partition-12 (Discrete) F₁score



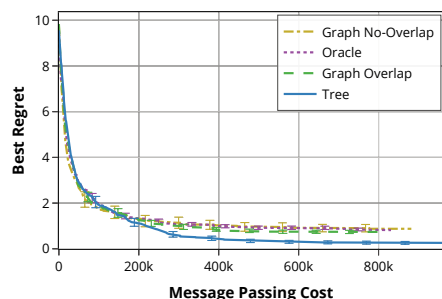
(i) Partition-12 (Discrete) Cost



(j) Grid-3×3 (Discrete) Performance

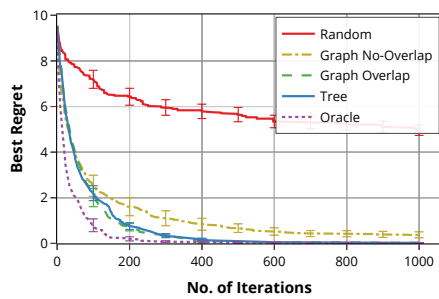


(k) Grid-3×3 (Discrete) F₁score

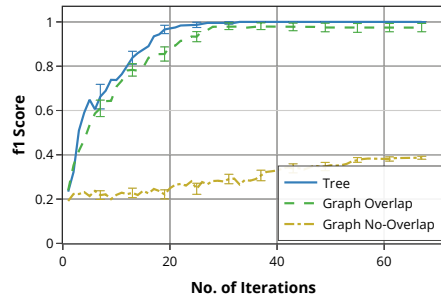


(l) Grid-3×3 (Discrete) Cost

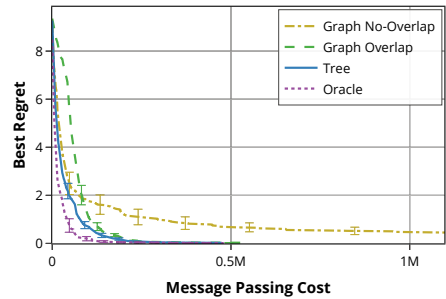
Figure S3: Results for synthetic additive functions on discrete domains.



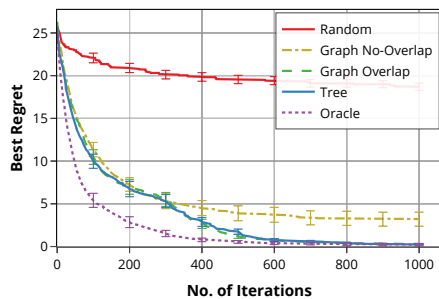
(a) Star-10 (Continuous) Performance



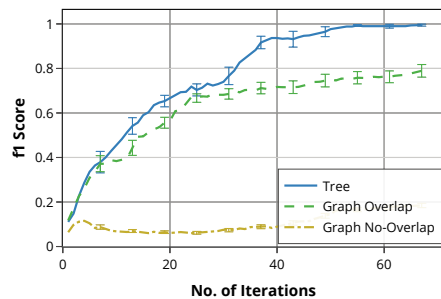
(b) Star-10 (Continuous) F₁score



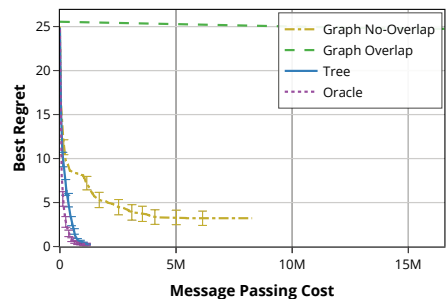
(c) Star-10 (Continuous) Cost



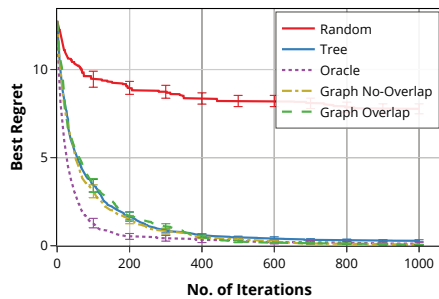
(d) Star-25 (Continuous) Performance



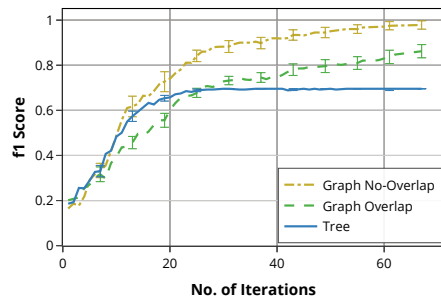
(e) Star-25 (Continuous) F₁score



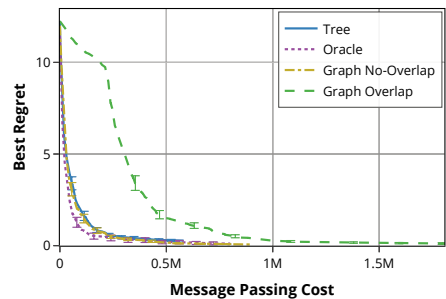
(f) Star-25 (Continuous) Cost



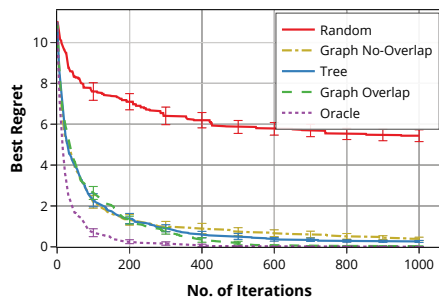
(g) Partition-12 (Continuous) Performance



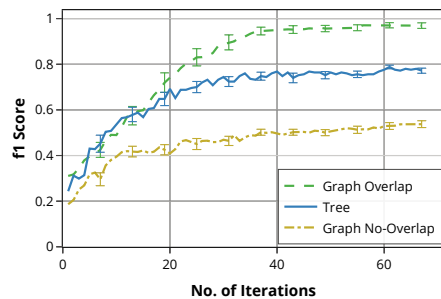
(h) Partition-12 (Continuous) F₁score



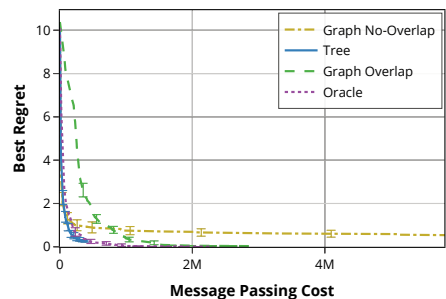
(i) Partition-12 (Continuous) Cost



(j) Grid-3 \times 3 (Continuous) Performance

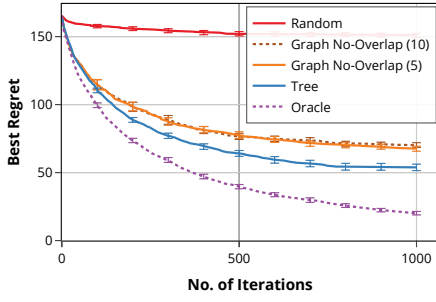


(k) Grid-3 \times 3 (Continuous) F₁score

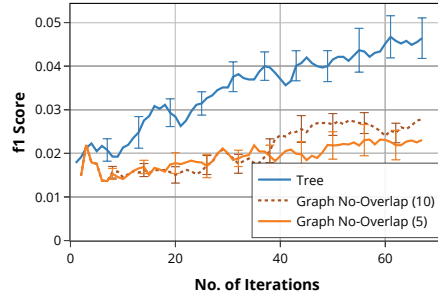


(l) Grid-3 \times 3 (Continuous) Cost

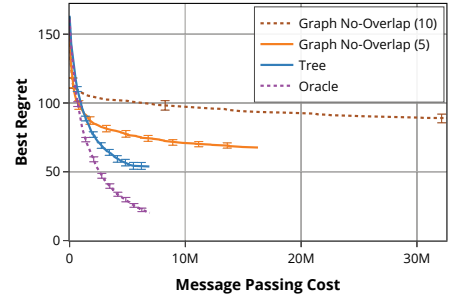
Figure S4: Results of synthetic additive functions on continuous domains.



(a) Ancestry-132 (Continuous) Performance

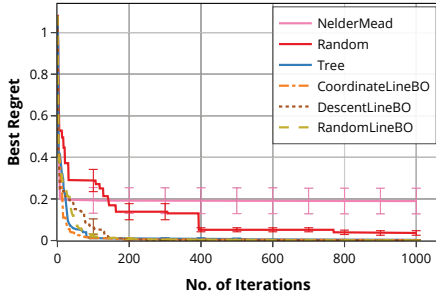


(b) Ancestry-132 (Continuous) F_1 Score

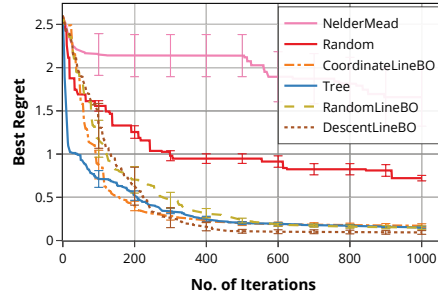


(c) Ancestry-132 (Continuous) Cost

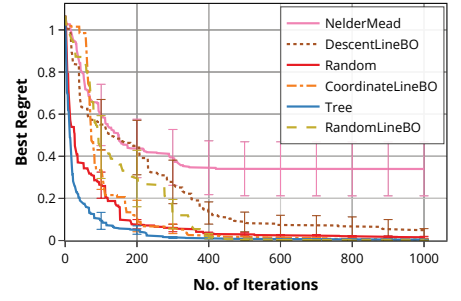
Figure S5: Results for the Ancestry-132 graph.



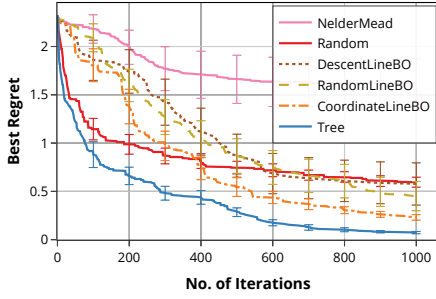
(a) Camelback2 Performance



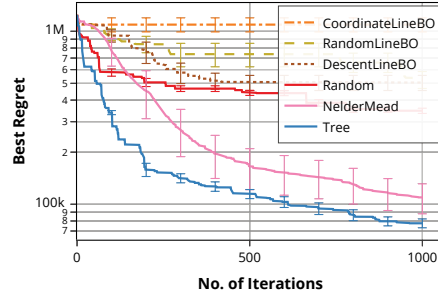
(b) Hartmann6 Performance



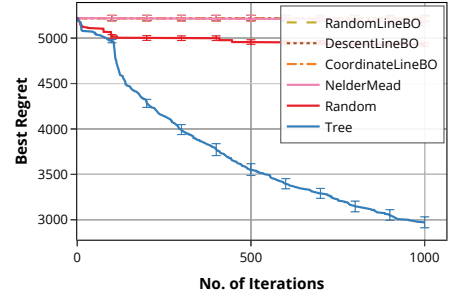
(c) Camelback2+10Aux Performance



(d) Hartmann6+14Aux Performance

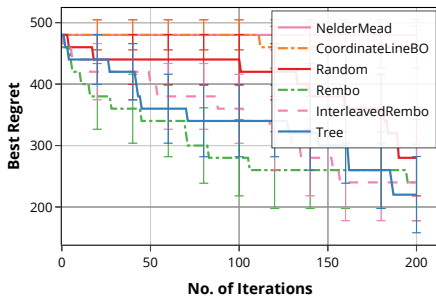


(e) Rosenbrock20 Performance

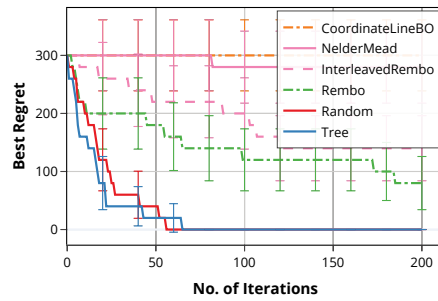


(f) Stybtang250 Performance

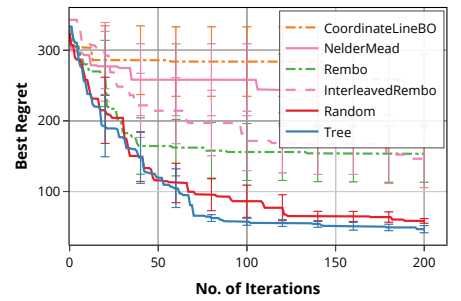
Figure S6: Results for non-GP synthetic functions.



(a) Lpsolve-misc05inf Performance

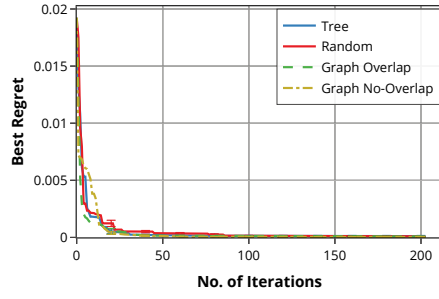


(b) Lpsolve-mtest4ma Performance

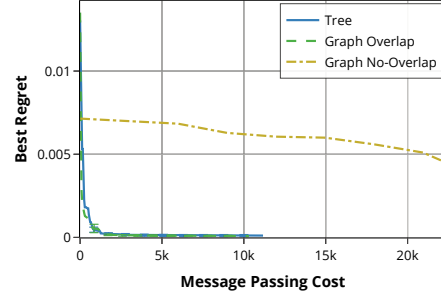


(c) Lpsolve-qiu Performance

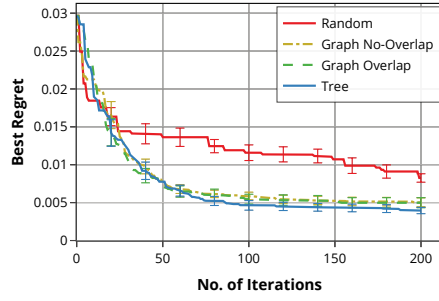
Figure S7: Results for Lpsolve hyperparameter tuning.



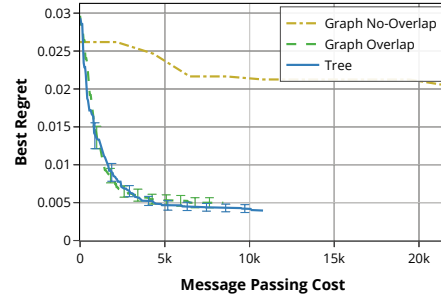
(a) NAS-naval Performance



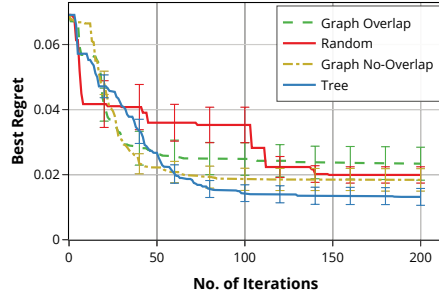
(b) NAS-naval Cost



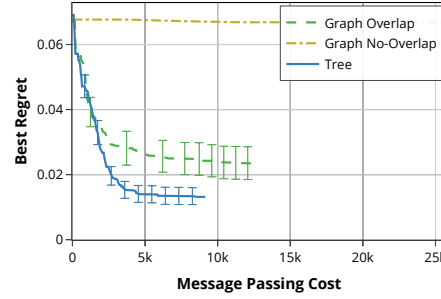
(c) NAS-parkinsons Performance



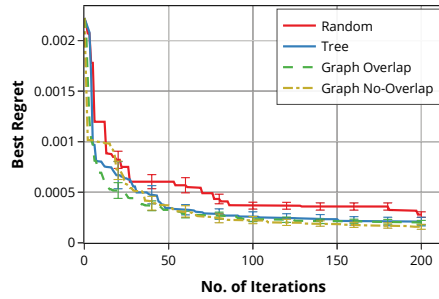
(d) NAS-parkinsons Cost



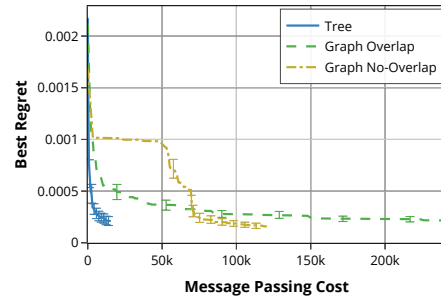
(e) NAS-protein Performance



(f) NAS-protein Cost

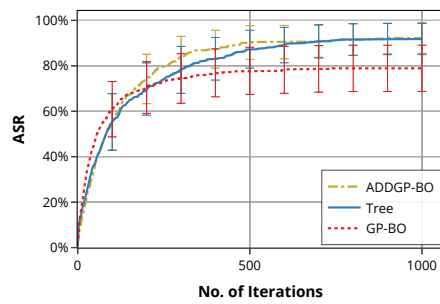


(g) NAS-slice Performance

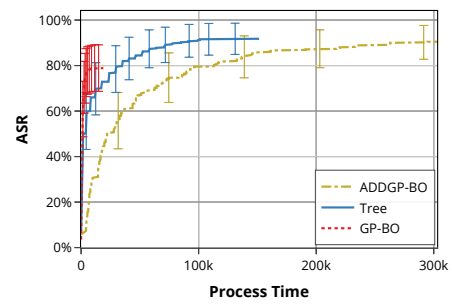


(h) NAS-slice Cost

Figure S8: Results for NAS-Bench-101 datasets.



(a) BA-MNIST Performance



(b) BA-MNIST Cost

Figure S9: Results for BO-based adversarial attacks.